Journal of Colloid and Interface Science 599 (2021) 140–148

Contents lists available at ScienceDirect

Journal of Colloid and Interface Science

journal homepage: www.elsevier.com/locate/jcis

Regular Article

Effect of the counter-ion on nanocellulose hydrogels and their superabsorbent structure and properties

Ruth M. Barajas-Ledesma [a], Laila Hossain [a], Vanessa N.L. Wong [c], Antonio F. Patti [b], Gil Garnier [a,*]

[a] Bioresource Processing Research Institute of Australia (BioPRIA) and Department of Chemical Engineering, Monash University, Clayton, VIC 3800, Australia
[b] School of Chemistry, Monash University, Clayton, VIC 3800, Australia
[c] School of Earth, Atmosphere & Environment, Monash University, Clayton, VIC 3800, Australia

GRAPHICAL ABSTRACT

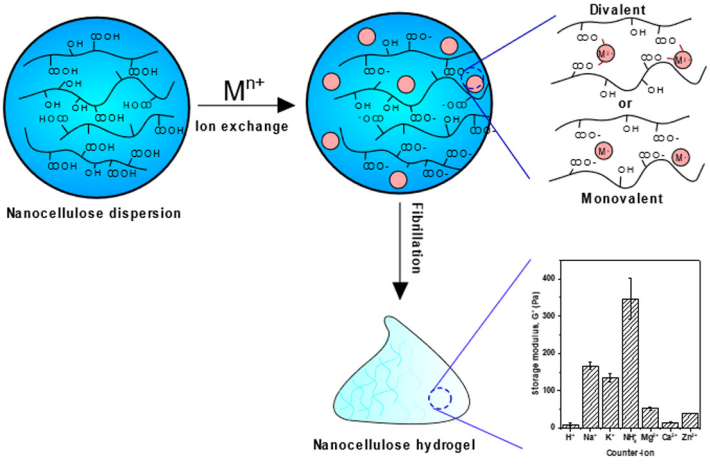

ARTICLE INFO

Article history:
Received 19 February 2021
Revised 12 April 2021
Accepted 13 April 2021
Available online 17 April 2021

Keywords:
Carboxylated nanocellulose
TEMPO
Cation
Valency
Superabsorbent
Gelation
Hydrogel
Foam
Aerogel

ABSTRACT

Hypothesis: Carboxylated nanocellulose gels and superabsorbents (SAPs) can be engineered by ion exchange of TEMPO treated cellulose fibers with different cations prior to shearing, thus creating a nanofibrous network ionically cross-linked. The structure and properties of these materials are highly influenced by the type counter-ion used as it controls both the degree of fibrillation and crosslinking.

Experiments: Functionalised nanocellulose SAPs were made using TEMPO-mediated oxidation followed by ion-exchange before fibrillation into a hydrogel and freeze-drying. Seven different cations were tested: 4 of valency 1 (H, Na, K, NH_4), and 3 of valency 2 (Ca, Mg, and Zn). The effect of the counter-ion on the gelation mechanism and the superabsorbent performance was evaluated. The SAP absorption capacity in deionised water was related to the superabsorbent structure and morphology.

Findings: The gel stability of nanocellulose superabsorbents is governed by the counter-ion type and valency. The viscoelastic properties of all nanocellulose hydrogels are controlled by its elastic regime, that is storage modulus (G′) > loss modulus (G″). The type of cation dictates the rheology of these gels by altering the fibrillation efficiency due to the extent of ionic cross-links occurring before and after fibrillation. The driving force for gelation in monovalent gels is due to the coupling of nanofibrils by physical interactions, creating an electrostatic stabilisation of the ionised COO^- groups at high shear forces. Cation – carboxylate interactions dominate the gelation in divalent gels by supressing the repulsive charges

* Corresponding author.
E-mail address: Gil.Garnier@Monash.edu (G. Garnier).

https://doi.org/10.1016/j.jcis.2021.04.065

generated by the COO^- and also creating interfibril connections via ionic-crosslinks, as confirmed by the zeta potentials. The superabsorption performance is dominated by the counter-ion and is in the order of: $NH_4^+ > K^+ > Na^+ > Mg^{2+} > Zn^{2+} > Ca^{2+}$. NH_4^+-SAPs present the slowest kinetics and the highest absorption capacity. Its high pore area, which extends the number of accessible carboxyl groups that participates in hydrogen bonding with water, is responsible for this behaviour. Nanocellulose SAPs are attractive renewable materials, suited for many applications, including as nutrient cation carriers in agriculture.

1. Introduction

Hydrogels are characterised by cross-linked networks of hydrophilic polymers that hold large amounts of water and remain stable [1–4]. The gelation mechanism is controlled by the density and type of cross-linking, physical or chemical. For physically cross-linked hydrogels, gelation is due to physical interacting forces such as van der Waals, hydrogen bonding, electrostatic and chain entanglements, among others [5]. Chemically cross-linked hydrogels undergo chemical reactions that covalently cross-linked the polymer network. These hydrogels are typically strong and permanent [5]. The formation of ionically-crosslinked hydrogels has been reported when metal salts are added to the polymer network, inducing gelation by screening repulsive charges [6,7].

Hydrogels can be used as superabsorbent polymers (SAPs) by removing the water of the network which, for nanocellulose, is often achieved by freeze-drying [8,9]. The resulting material from freeze-drying appears as a foamy-like structure, also referred to as nanocellulose foam or aerogel [8,10]. Their swelling is dictated by the movement of the counter-ions from outside to inside the superabsorbent, causing an osmotic pressure difference across the network [11]. These materials are found in numerous applications such as hygiene and personal care products [12]. agriculture [13] and biomedicine [14]. In agriculture, SAPs can act as soil conditioners, increasing plant water availability and soil water retention [15,16], and as slow release fertilisers or nutrient carriers [16].

The majority of the available superabsorbents are fossil fuel derived polymers which degrade slowly and raise health and environmental concerns due to the formation of microplastic particles that can be harmful to soil biota [17–19]. These environmental issues have driven the development of superabsorbents from natural polymers, especially those made of starch [20], pectin [21], alginate [22], or cellulose [23,24]. From these, cellulose, the most abundant carbohydrate and biopolymer on earth, is often preferred as source material due its biodegradability, availability and hydrophilicity [16,25]. Cellulose-based SAPs can be produced through the 2,2,6,6-tetramethylpiperidine-1-oxyl (TEMPO)-mediated oxidation of cellulose followed by (freeze)drying. This process converts the primary alcohol groups of cellulose into sodium carboxylate groups [26]. and adds the required electrostatic repulsion which forms nanocellulose hydrogels upon mechanical fibrillation. Nanocellulose-based SAPs are regarded as highly-porous materials with high swelling and water retention properties [8,27].

The sodium ions present in the polymer matrix is not desirable for agricultural related applications of nanocellulose superabsorbents. Adding sodium to soils will have an adverse effect on soil structure, oxygen and water availability and can impose a stress on growing crops, resulting in a decrease of yields or crop failure [28]. The exchange of the counter-ion with others can tailor this material not only as a superabsorbent, but also as a nutrient carrier for plants. Literature suggests that the cation can significantly influence the properties of cellulose-based materials. Homma, Fukuzumi, Saito and Isogai [29] found that the biodegradation rate of TEMPO-oxidised nanofibril films is greatly influenced by the counter-ion; Na^+ are reported to have the fastest rate and Cu^{2+} the lowest. Dong, Snyder, Williams and Andzelm [6] revealed that the storage modulus (G') of cellulose nanofibril hydrogels increase with increasing valency of the metal cation and are strongly associated to the binding energy of the COO^- groups with the nanofibers. Yang, Xu and Han [7] showed that cellulose nanofibers (CNF) covalently cross-linked with polyacrylamide (PAAm) can be reinforced with multivalent cations to create hydrogels of high stiffness and toughness. The addition of these ionic-links between the metal cation and CNF improves hardness and elasticity by 600% compared to pristine gels.

Ionically cross-linked nanocellulose hydrogels can be prepared by subjecting the TEMPO-oxidised nanocellulose to an aqueous salt solution before or after fibrillation, with most of the studies using the latter. This technique consists on adding the salt solution dropwise to a dispersion of TEMPO-oxidised cellulose nanofibers, without stirring, which are left standing overnight [6,7,30,31]. This process selectively substitutes the sodium ions present in the dispersion with another ion of stronger affinity. However, this technique is not only slow – which can sometimes take up to 5 days [30]- but also challenging to scale up, thus limiting the application range.

While several studies investigated the effect that different metal cations have on the gelation of nanocellulose-based hydrogels, none have studied the effect of the different cations on the viscoelastic properties of nanocellulose hydrogels nor associated those to the superabsorption performance. Similarly, while some studies suggested that the addition of salt solution after fibrillation results in the formation of heterogenous clumps and the loss of the gel structure [32]. the effect of the cation on the fibrillation efficiency upon homogenisation is unknown.

Here, TEMPO mediated oxidation was used to prepare carboxylated nanocellulose hydrogels. The oxidised fibres were subjected to an acid wash with HCl to remove all Na^+ cations present, followed by fibre re-suspension in different salt solutions, homogenisation and freeze-drying. The fibrillation efficiency, hydrogel rheology and SAP structure and swelling properties were measured. This study innovates by the technique used to prepare ionically cross-linked SAPs. The addition of these cations can not only assist in the transition of the superabsorbent as a hydro-retentor material to a nutrient carrier material for applications in sustainable agriculture, but also help in understanding the behaviour of superabsorbent in soils where there is a natural mixture of exchangeable cations, including Ca^{2+}, Mg^{2+} and K^+.

2. Materials and methods

2.1. Materials

Bleached Eucalyptus Kraft (BEK) pulp was provided by Australian Paper, Maryvale, Australia with a chemical composition of cellulose (78.8% ± 0.8), hemicellulose (17.7% ± 0.4), lignin (3.2% ± 0.1), extractives (0.3% ± 0.1) and ash (0.2% ± 0.1) [33]. Sodium hypochlorite (NaClO) at 12% w/v was purchased from Thermo Fisher Scientific and used as received. 2,2,6,6-Tetramethylpiperi

dine-1-oxyl (TEMPO) and Sodium bromide (NaBr) were purchased from Sigma-Aldrich. Sodium hydroxide (NaOH) and hydrochloric acid (HCl) were purchased from ACL Laboratories and Merck, respectively, and diluted for solutions as needed. Zinc sulfate monohydrate ($ZnSO_4{\cdot}H_2O$), sodium sulfate anhydrous (Na_2SO_4), ammonium sulfate ($(NH_4)_2SO_4$) and potassium sulfate (K_2SO_4) were purchased from Sigma-Aldrich. Calcium sulfate hemihydrate ($CaSO_4.½H_2O$) and Copper (II) sulfate pentahydrate ($CuSO_4{\cdot}5H_2O$) were purchased from Westlab. Magnesium sulfate anhydrous ($MgSO_4$) was purchased from Merck. 70% Nitric acid (HNO_3) was purchased from Ajax Finechem.

2.2. Synthesis of carboxylated cellulose

The oxidation process was based on a previously developed method [26]. In brief, 25 g of BEK pulp (dry basis) was dispersed in 2500 mL of water with 2.5 g and 0.4 g of dissolved sodium bromide and TEMPO, respectively. Prior to the oxidation process, the sodium hypochlorite at 12% w/v was adjusted to pH 10 through the addition of hydrochloric acid at 36% w/v. To achieve a carboxylate content of 1.4 mmol/g of dry fibre, 100 mL of sodium hypochlorite was added drop-wise to the suspension whilst stirring. The pH of the reaction was maintained at 10 by adding 0.5 M NaOH. The reaction was complete when the change in pH was negligible. The oxidised cellulose was washed with deionised water, filtrated and stored refrigerated at 4 °C until required. The sodium carboxylate content of the TEMPO oxidised cellulose was 1.4 mmol/g dry fibre and was measured by conductivity titration [34].

2.3. Ion exchange treatment of carboxylated cellulose

The ion exchange treatment employed was based on a previously reported method [29]. 1 g of the TEMPO-oxidised fibres, containing sodium carboxylate groups, was suspended in 1 L of 0.01 M HCl and stirred for 1 h. The oxidised cellulose pulp was later washed with Milli-Q water and filtrated. The oxidised pulp with protonated carboxyl groups was then re-suspended in 1 L of salt solution and stirred for 3 h at room temperature. The number of moles of salt dissolved in the suspension was fixed to be 10 times as much as the calculated carboxylate groups present in the oxidised cellulose. After 3 h, the salt treated cellulose fibres were washed with Milli-Q water, filtrated and stored refrigerated at 4 °C until required. The following solutions were used for the ion-exchange treatment: hydrochloric acid (HCl), sodium sulfate (Na_2SO_4), zinc sulfate ($ZnSO_4$), potassium sulfate (K_2SO_4), ammonium sulfate ($(NH_4)_2SO_4$), copper (II) sulfate pentahydrate ($CuSO_4$), calcium sulfate ($CaSO_4$), magnesium sulfate ($MgSO_4$). Sulfate anion salts were selected to negate the effect of the anion and for its suitability for agriculture.

2.4. Preparation of nanocellulose hydrogel and superabsorbent

To prepare the nanocellulose hydrogel, the TEMPO-oxidised fibres treated with the various counter-ions were suspended in Milli-Q water to achieve a concentration of solids of 0.5% w/v and fibrillated through high pressure homogenisation (GEA Niro Soavi Homogeniser Panda) at 800 bar and two passes. To produce the nanocellulose superabsorbent, the resulting hydrogel from homogenisation was stored for at least 12 h at −80 °C and freeze-dried for 48 h using a Christ Alpha 2–4 LD Plus.

2.5. Characterisation

Freeze-dried nanocellulose SAP was characterised using a Fourier Transform Infrared (FTIR) spectrometer (Agilent Technologies Cary 630 FTIR).

The counter-ion content in nanocellulose hydrogels was analysed by either elemental analysis (HCNS) using a Perkin Elmer 2400 Series II analyser, for NH_4^+ and H^+ gels, or by inductively coupled plasma – optical emission spectrometry (ICP-OES), for all other ions. For ICP-OES analysis, 3 g of nanocellulose hydrogel was placed in crucibles and ashed using a muffle furnace, based on a previously reported method [35]. Temperature ramped to 600 °C over 3 h and kept for a further 3 h. The metal residues left in the crucible were dissolved using 1 mL of 70% HNO_3 and diluted with Milli-Q water to achieve a total volume of 15 mL. The dissolved metals were then analysed by ICP-OES using a Perkin-Elmer Avio 200. Each sample was analysed in triplicate.

The zeta potential of the nanocellulose hydrogels was measured following the method described by Mendoza, Hossain, Browne, Raghuwanshi, Simon and Garnier [36]. Briefly, 1 mL of each salt treated gel was diluted to a concentration 0.01% and sonicated using an ultrasonic homogeniser at 70% amplitude (ON/OFF, 5 s) and 19.5 kHz for 2 min. Large cellulose fibres were removed by centrifugation for 5 min at 4400 rpm. The zeta potential was measured using a Brookhaven Nanobrook Omni. Each sample was analysed 5 times.

The viscoelastic properties of nanocellulose hydrogels were evaluated using a rheometer (Anton Paar MCR302) at 25 °C. A cone (0.997°) and plate (49.975 mm) geometry was selected for Na^+, K^+ and NH_4^+ and a cup and bob for H^+, Mg^{2+}, Ca^{2+} and Zn^{2+} ions. During the measurements, a solvent trap was employed to maintain a constant temperature. The amplitude sweep was varied from 0.01 to 100% at a constant frequency of 1 Hz.

The morphology of the SAPs was observed using scanning electron microscopy (SEM) (FEI Magellan 400). Nanocellulose foams were placed on a metal stub and coated with an Iridium layer of less than 2 nm thick.

The porosity, pore size distribution and pore properties of all SAPs were measured by mercury porosimetry (Micromeritics Autopore IV). Samples were degassed at 50 °C for at least 24 h prior testing and analysed in triplicates. The testing pressure ranged from 0.1 to 60,000 psia was applied.

The swelling or absorption capacity of nanocellulose SAPs was quantified in Milli-Q water. The swelling rate and absorption were measured by weighing the samples before and after immersion in water over different periods of time (1, 5, 15, 30, 60, 90, and 150 min) at room temperature. The following equation was used to determine the swelling capacity:

$$Swelling\ \ capacity, Q = \frac{m_t - m_d}{m_d} \quad (1)$$

where m_t refers to the weight of the swollen gel at time t and m_d is the weight of the dried sample.

3. Results

TEMPO oxidised BEK pulp, which had a carboxylate content of 1.4 mmol/g dry fibre and was washed with acid, was first dispersed into different salt solutions of varying valency and cation type and then homogenised under high shear forces, thus forming hydrogels. These hydrogels were characterised in chemical structure and ion content. Rheology was used to evaluate the cross-linking density and fibrillation efficiency. Hydrogels were then lyophilised and the aerogels produced were analysed for morphology, pore size distribution and swelling in water.

3.1. Ion exchange of carboxyl-group counter-ions

The FT-IR spectra and the zeta potential of the hydrogels prepared with the various counter-ions is displayed in Fig. 1a and b, respectively. The presence of a band at 1720 cm^{-1} for the H^+-hydrogel indicates the conversion of the Na^+ carboxylate groups from the TEMPO-mediated oxidation to carboxylic acid groups using the acid treatment (Fig. 1a). All samples with monovalent ions (Na^+, K^+ and NH_4^+) and divalent ions (Mg^{2+}, Ca^{2+} and Zn^{2+}) show a sharp peak at 1600 cm^{-1}, distinctive of the C=O stretching groups, which confirms the presence of the carboxylate functional group which will be associated with the respective counter-ions. Interestingly, the zeta potential of the nanocellulose hydrogels decreased with increasing ion valency. Monovalent hydrogels have a zeta potential ranging from −80 mV to −74 mV; for divalent, it ranges from −50 to −35 mV. Ca^{2+}-hydrogels have the lowest surface charge of all samples (Fig. 1b). The difference between and among the valencies is significant, as previously reported [37].

The degree of counter-ion exchange from the protonated carboxyl group to other cations was evaluated through ICP-OES analysis (Fig. 2). NH_4^+ ions were determined by HCNS analysis, also shown in Fig. 2. Except for Zn^{2+}-gels, the measured counter-ion content of all ions is similar to that calculated by stoichiometry – 1.4 and 0.7 mmol/g dry fibre for mono and divalent cation gels, respectively. This confirms the complete conversion of the protonated carboxyl groups to their respective carboxylate salt. Samples with divalent ions formed cationic carboxylate groups with 1:2 (cation-COO) molar ratio, corresponding to $(COO)_2$-cation structures ionically cross-linked. The increase in the measured counter-ion content of Zn^{2+}-gels higher than the calculated value can be attributed to an excess of salt solution that was not completely removed upon washing.

3.2. Viscoelastic properties

The effect of the counter-ions on the gelation properties of the nanocellulose hydrogels was measured by rheology. The viscosity curves of all gels are presented in Fig. 3a. In general, increasing shear rate decreases viscosity. This is known as a shear-thinning behaviour and is common in nanocellulose gels [38,39]. Gels with divalent ions have lower shear viscosity than those with monovalent ions.

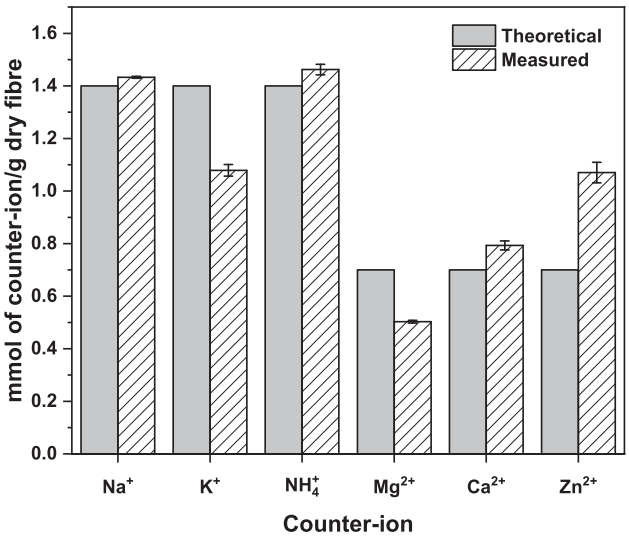

Fig. 2. Counter-ion content of the TEMPO-oxidised nanocellulose sheared after the ion exchange treatment. Measurements are determined from ICP-OES and HCNS analysis. Results are reported as mean ± standard deviation (n = 3).

The storage modulus or solid-like behaviour (G') and the loss modulus or liquid-like behaviour (G'') were evaluated as a function of shear strain in oscillatory flow mode (Fig. 3d-e). The viscoelastic properties of the nanocellulose gels is governed by the elastic regime in all cases, noted by a higher G' than G'' over the strain range. The storage modulus of the gels decreases with increasing ion valency. Monovalent gels, except those with H^+ ion, exhibit an elastic modulus an order of magnitude higher than all divalent ions providing an indication of fibre crosslinking in between the gel matrix [7]. Gel stiffness, described by the G' values (Fig. 3b), is in the order of $NH_4^+ \gg Na^+ > K^+ > Mg^{2+} > Zn^{2+} > Ca^{2+} > H^+$. Similarly, gel relaxation, described by G'' values (Fig. 3c), is in the decreasing order of $NH_4^+ \gg Na^+ > K^+ > Mg^{2+} > Ca^{2+} \sim Zn^{2+} > H^+$. The linear viscoelastic region (LVR) changes for both curves, G' and G'', depending on the valency and type of counter-ion. Both hydrogels display a similar LVR regime that drops at a shear strain of 10%. Finally, the difference between the G′ and the G″ values for monovalent gels is an order of magnitude higher than for divalent

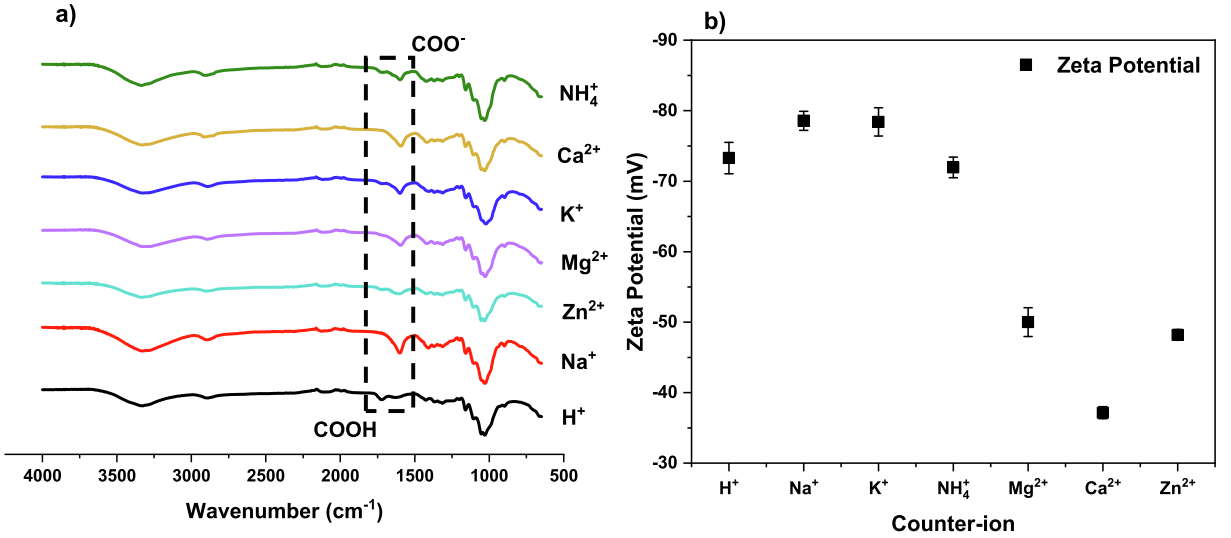

Fig. 1. (a) FT-IR spectra and (b) zeta potential of TEMPO-oxidised nanocellulose pretreated with different counter-ions. The dashed line highlights the absorption bands for COO– and COOH groups. Results are reported as mean ± standard deviation (n = 3).

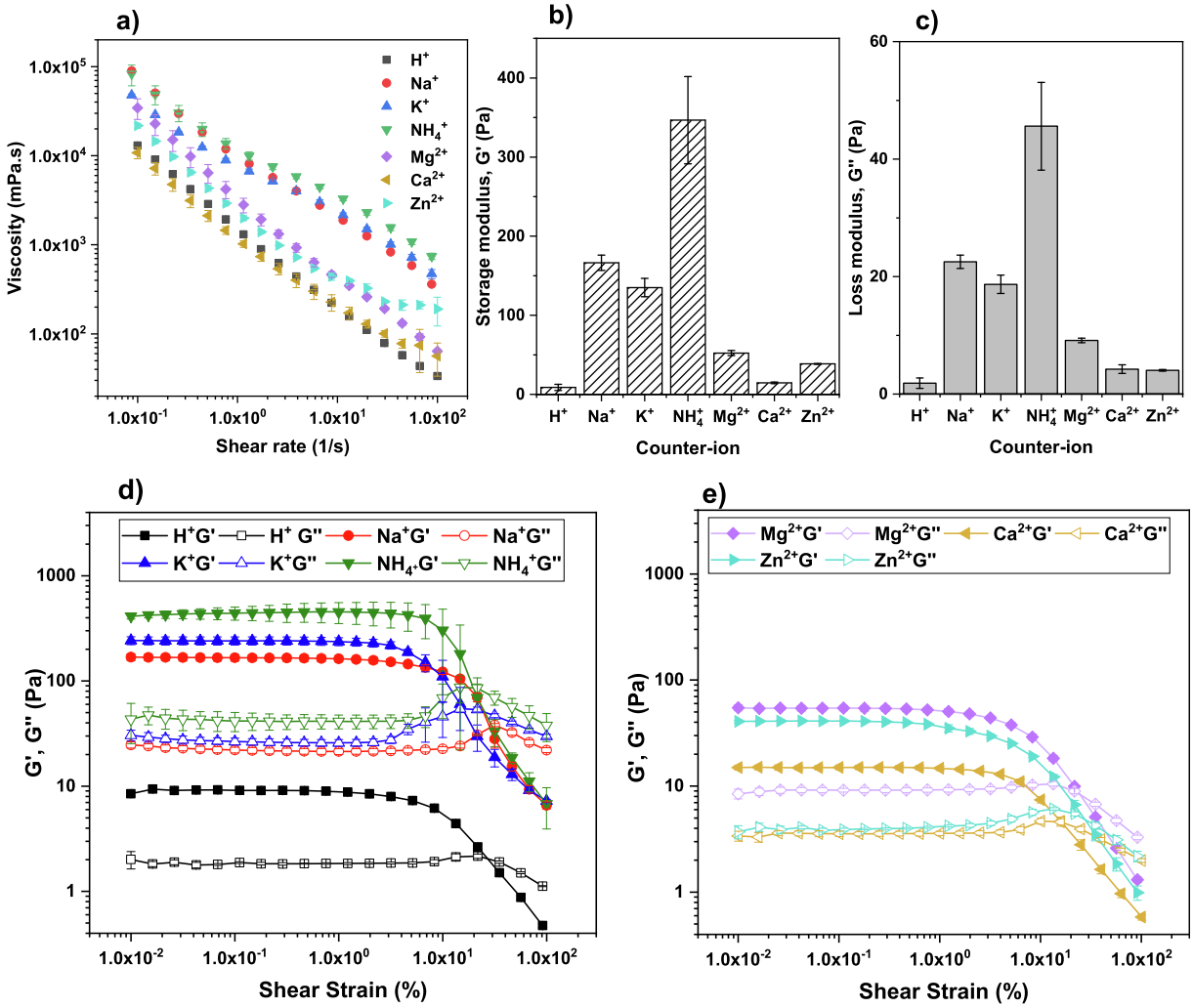

Fig. 3. Rheological properties of TEMPO-oxidised nanocellulose sheared with different counter-ions: (a) viscosity curves, (b) nanocellulose gel stiffness and (c) relaxation represented by the storage modulus (G') and the loss modulus (G''), storage (G') and loss (G'') modulus of (d) monovalent and (e) divalent ions. Results are reported as mean ± standard deviation (n = 3).

gels. This suggests that monovalent gels are mostly dominated by the elastic character, whereas divalent and H^+ gels are dictated by both the elastic and the viscous behaviour in the same proportion.

3.3. Morphology

Nanocellulose-based aerogels were prepared by freeze-drying. SEM imaging was employed to analyse the morphology (Fig. 4). The internal structure strongly depends on the counter-ion present in the superabsorbent. Though all treatments produced SAPs with very porous structures, the pore shape, size and fibre arrangement differ. Monovalent ions form SAPs characterised by an entanglement of fibres which results in open and porous three-dimensional assemblies (Fig. 4a-d). Fibres are clearly visible, forming foam structures with pore diameters ranging from 10 to 300 nm. In contrast, superabsorbents with divalent ions are characterised by a more homogeneous and organised structure. Pores are detected, but the cellulose fibres are still connected to each other, not entangled (Fig. 4e-g). Pore diameters range between 30 and 200 nm.

3.4. Pore size

The pore size distribution of the nanocellulose superabsorbents was evaluated using mercury porosimetry (Fig. 5a). Pore size distribution is controlled by the counter-ion present in the SAP. Apart from NH_4^+, all monovalent and divalent ions form SAP with a microporous structure. No visible pores are noted at a scale lower than 2 μm. Superabsorbents made with NH_4^+ counter-ion display a combination of micro, *meso* and macropores of size ranging from 5 nm to up to 100 μm, classified by IUPAC [40].

The pore properties of the superabsorbents is expressed as a function of the counter-ion (Fig. 5a-c). NH_4^+-based superabsorbents exhibit the highest pore area, more than 15 times higher than any of the other SAPs. It also has the smallest pore diameter, in the range of 2–5 nm, which is about 6 times smaller than for the other materials. Apart from this, there are no other major difference observed in the SAPs prepared with the other monovalent and divalent ions. The pore volume is slightly smaller for superabsorbents with monovalent ions than for divalent ions, ranging from 25–30 mL/g and 32–37 mL/g, respectively. The porosity of all the SAPs is in between 90 and 94%, which is typical of freeze-dried superabsorbents [8].

3.5. Swelling

The degree of swelling of the nanocellulose SAPs was quantified in Milli-Q water and evaluated as over time (Fig. 6). All superabsorbents perform similarly, with swelling uptake reaching a plateau after an initial absorption rate. Apart from NH_4^+,

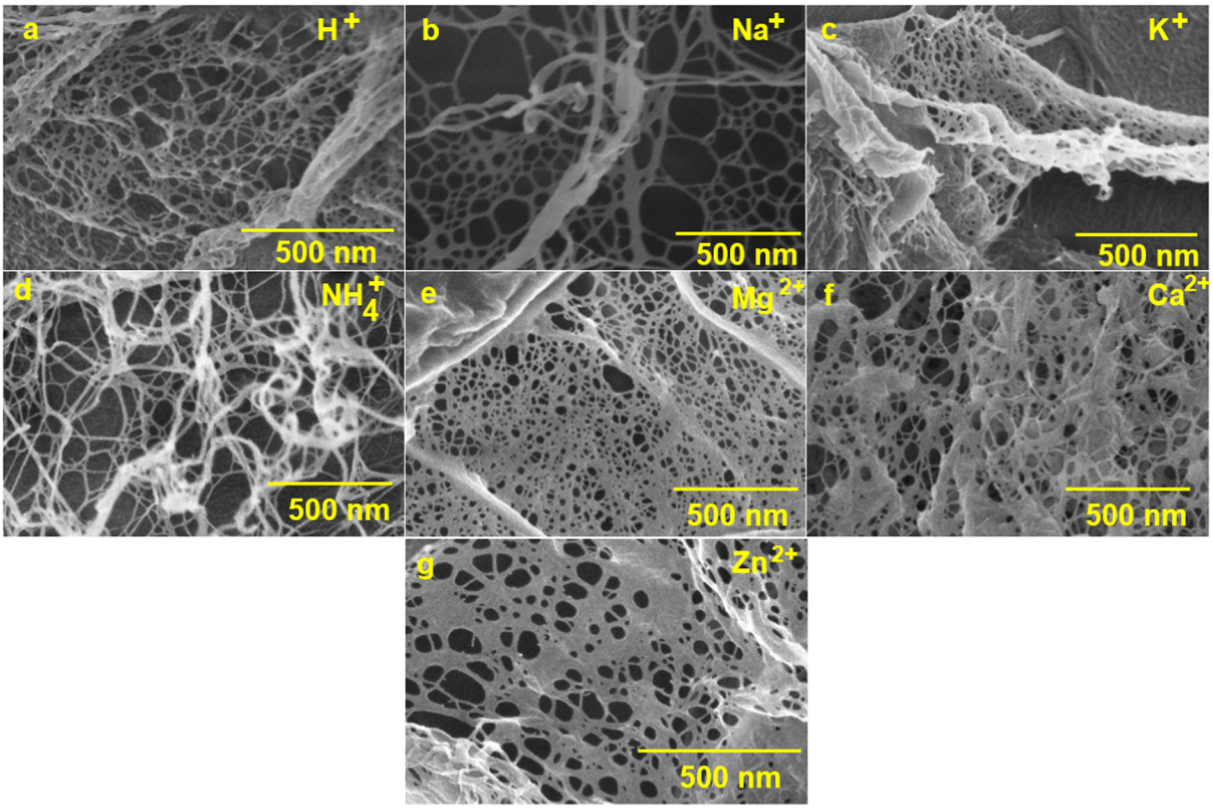

Fig. 4. SEM images of the nanocellulose superabsorbent made from freeze-drying nanocellulose hydrogels of TEMPO-treated cellulose sheared with different counter-ions: (a) H^+, (b) Na^+, (c) K^+, (d) NH_4^+, (e) Mg^{2+}, (f) Ca^{2+} and (g) Zn^{2+}.

superabsorbents show an initial rapid swelling, achieving equilibrium as soon as they are immersed in water. SAP with NH_4^+ counter-ion is characterised a slow swelling rate.

The type of counter-ion dictates the SAP swelling at equilibrium (Fig. 7). Ammonium-based SAP achieves the highest swelling capacity of approximately 130 g water/g dry fibre. This is followed by the other monovalent ions, K^+ and Na^+, in order, respectively. SAPs with valency two ions report a lower swelling capacity, with Ca^{2+} being the lowest of all.

4. Discussion

TEMPO-mediated oxidation is the most commonly used method to produce nanocellulose hydrogels. This introduces sodium carboxylates at the C6 glycosidic position which contributes to the liberation of cellulose fibres upon homogenisation. However, the presence of sodium counter-ions may limit the application range of this material. This study evaluated the effects that different counter-ions have on the properties of both nanocellulose hydrogels and superabsorbents via ion exchange treatment prior fibrillation.

The FT-IR spectra analysis confirms the evidence of the carboxylate groups balanced by different cations or protonated carboxyl groups. This is noted by the presence of their characteristic peak of metal carboxylate group at ~1600 cm^{-1}. However, the intensity of this peak is lower for hydrogels with Zn^{2+} and NH_4^+ ions. In these cases, the FT-IR spectra also show a small peak at ~1720 cm^{-1} which corresponds to protonated carboxyl groups. This suggests that not all the carboxyl groups were converted to the corresponding metal carboxylate group [29,41]. This is because of the pH of $ZnSO_4$ and NH_4SO_4 solutions being 4.8 and 5.5 respectively, which promotes the partial formation of free carboxylic acid.

Except for Zn^{2+}-gels, the addition of multivalent ions forms cation carboxylate groups with molar ratios of 1:1 and 1:2 for monovalent cations (NH_4^+, H^+, Na^+, K^+) and divalent cations (Zn^{2+}, Ca^{2+}, Mg^{2+}), respectively. Divalent cations have a higher solvation volume and binding energy than monovalent cations which allows interfibril interactions, leading to ionic cross-linking between multiple fibres [6]. These ionic links generate strong interactions with numerous carboxylate groups, bridging cellulose nanofibers by attractive forces that screen the electrostatic repulsion between neighbouring nanofibres [7]. This screening effect governs the gel stability and increases with increasing concentration and counter-ion valency [42]. This is confirmed with the surface charge of the hydrogels, being almost half that of monovalent gels, indicating the formation of significant cohesive interactions between nanofibrils due to the strength of these interfibril connections [6]. The surface charge, measured by zeta potential, is related to the physical stability of these gels by electrostatic repulsion of individual fibres. Values higher than +/−30 mV can develop enough repulsive force to reach good colloidal stability. On the other hand, smaller values can lead to flocculation and particle aggregation [43]. In this case, the low zeta potential values of divalent gels, with Ca^{2+}-gels being close to the threshold of agglomeration, led to a decrease in the degree of nanofibrillation, exhibited by the substantial fibril aggregation observed in the nanocellulose dispersion after fibrillation and in the morphology of the aerogels upon drying (Fig. 4) [36]. Fibril aggregation was also observed in gels with H^+ ions. In this case, gel stability is governed by the protonated carboxyl groups which decrease the electrostatic repulsion and surface charge, allowing the fibres to come closer as the van

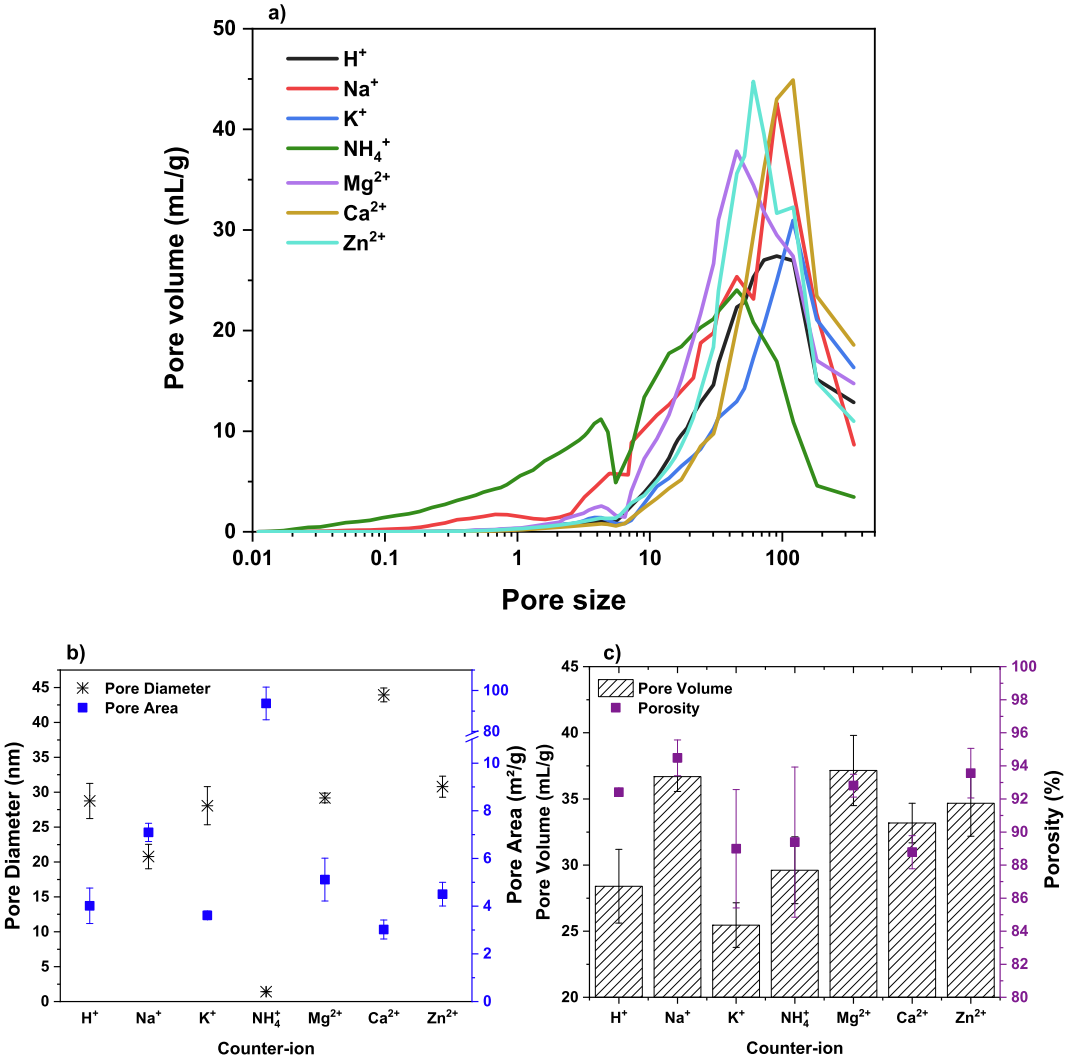

Fig. 5. Pore properties of the nanocellulose superabsorbents with different counter-ions: (a) pore size distribution (b) pore diameter and pore area, and (c) porosity and pore volume. Results are reported as mean +/− standard deviation (n = 3).

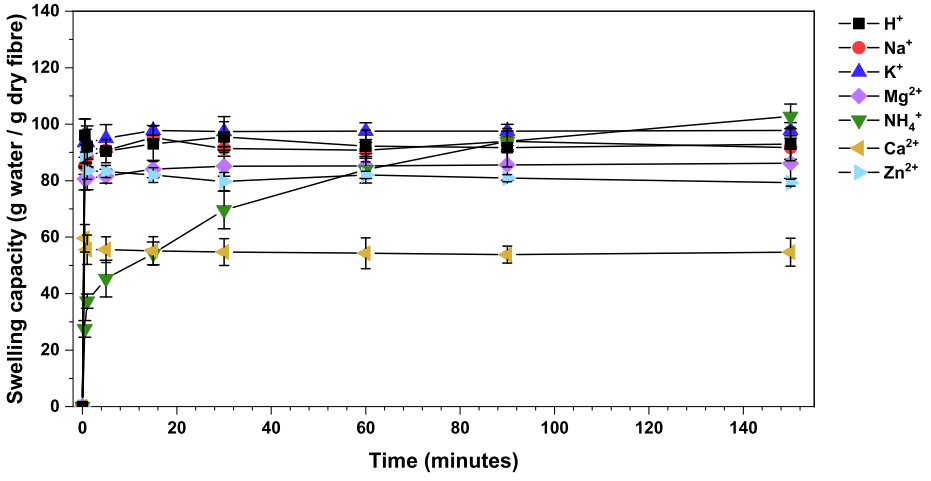

Fig. 6. Effect of the counter-ion on the degree of swelling of nanocellulose superabsorbents over time. Results are reported as mean ± standard deviation (n = 3).

der Waals forces become dominant, resulting in a decrease in the degree of fibrillation [32,44]. In contrast, monovalent ionic gels lack the interfibril cross-linking interactions as observed with the viscoelastic properties. Thus, the driving force for gelation is due to the coupling of nanofibrils by physical interactions that creates an electrostatic stabilisation of the ionised COO^- groups when high

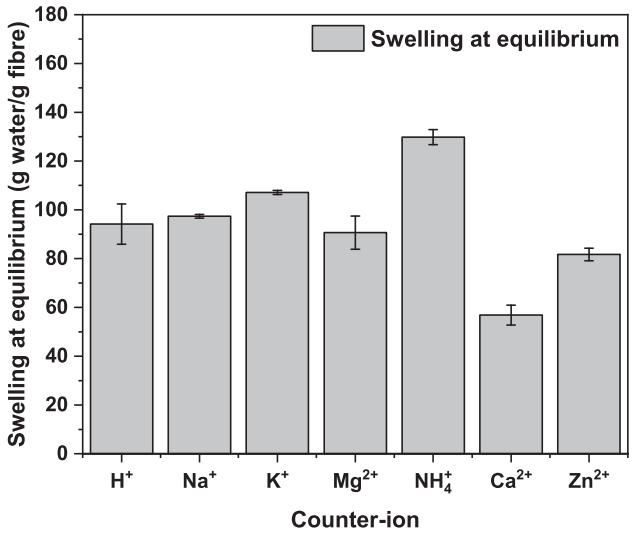

Fig. 7. Effect of the counter-ion on the swelling capacity of nanocellulose superabsorbents at equilibrium. Results are reported as mean +/- standard deviation (n = 3).

shear forces are applied to the oxidised fibres [6,32], forming stronger and more stable materials.

The type of counter-ion governs the superabsorption performance. The interaction of the counter-ion with the cellulose nanofibers can be explained by two main variables. For monovalent ions, the swelling at equilibrium follows the Hofmeister effect. This effect relates the behaviour of hydrophilic colloids in the presence of salts and is attributed to the size and hydration of ions [45]. According to the Hofmeister effect, stability of hydrophilic particles follows the indirect series as: $NH_4^+ > K^+ > Na^+$. Where ions on the left will adsorb more strongly to a hydrophilic substrate [45]. This cation specificity coincides with the measured values of swelling capacity and is attributed to negative volume exclusion entropy generated by the cation hydration. This results in an increase of the strength of the electrostatic repulsive forces which increases the entanglement of nanocellulose fibres [46,47]. Thus, increasing the absorption capacity due to the increase in hydrogen bonding between the COO^- available to interact with water [48] and also contributing to the swelling of the fibre network [10].

These repulsive forces are screened in the presence of divalent cations, as van der Waals forces become dominant and strong cation-carboxylate bonds are created [6]. Cellulose nanofibers come closer, decreasing the fibre ability to entangle upon fibrillation and thus, decreasing the swelling capacity. In this case, swelling is mainly attributed to the available pore volume, where swelling increases with increasing pore volume and decreases in the order of $Mg^{2+} > Zn^{2+} > Ca^{2+}$. This difference in pore volume depending on the counter-ion can be associated to the cation radii, where the increment in ionic radii of valency two cations results in a decrease in swelling (Mg^{2+} (72 pm) < Ca^{2+} (100 pm)) [49].

Lastly, of all the cations studied, NH_4^+ produced gels and superabsorbents with remarkable properties: high gel stiffness and stability, high SAP pore area and swelling, and slow swelling kinetics. Such performance is attributed to the unique ability of the ammonium cation to rotate [50]. This ability creates additional hydrogen bonds between the water molecules and the nanofiber network, resulting in a higher fibrillation efficiency upon homogenisation. This increase in fibre entanglement is observed in the small pore size and wide pore distribution of this SAP (Fig. 4d, 5a and 5b), increasing the pore area by an order of magnitude. This expands the number of available carboxyl groups able to participate with hydrogen bonding, resulting in a high gel stiffness. This also increases the swelling of the nanofibre network and the amount of water adsorbed to the polymer chains, responsible for the high swelling of this superabsorbent [51].

5. Conclusion

A number of nanocellulose hydrogels varying in the extent of cellulose fiberization and ion cross-linking was prepared and freeze-dried into superabsorbents (SAP). Gel and SAP were characterized in terms of rheology, aerogel structure, gelation mechanism and swelling behaviour. Carboxylated nanocellulose was prepared from TEMPO oxidized cellulose followed by ion exchange in a series of salt solutions prior to high shear homogenization into a gel [10]. Seven cations were ion exchanged to the COO^- groups. These are: H^+, Na^+, K^+, NH_4^+, Ca^{2+}, Mg^{2+} and Zn^{2+}; the anion was sulfate. The effect of the cation on the gelation properties and mechanism, superabsorbent structure, swelling capacity and absorption rate was analysed.

FT-IR and ICP-OES analyses confirm the formation of metal carboxylate groups with 1:1 (metal-COO) molar ratio for monovalent cations and 1:2 M ratio for divalent cations, which corresponds to $(COO)_2$-metal structures ionically cross-linked. The gel stability of the nanocellulose is governed by the valency and the type of cation. Gelation in monovalent gels is due to the coupling of nanofibrils by physical interactions which creates an electrostatic stabilisation of the ionised carboxyl groups during the high shear forces of homogenizing [6,32]. In contrast, for divalent gels, the driving force for gelation is due to strong interfibril connections via ionic-crosslinks which screen the repulsive forces between carboxylate groups, enabling fibres to associate together. The type of ion and their interaction with the COO^- groups determine the efficiency of fibrillation during homogenization, which affects the structure of the hydrogels and aerogels made of those. This aerogel structure directly impacts swelling capacity and kinetics. Swelling at equilibrium is in order of: $NH_4^+ > K^+ > Na^+ > Mg^{2+} > Zn^{2+} > Ca^{2+}$. The swelling capacity of monovalent SAPs follows the Hofmeister effect and is related to the size and hydration of ions. For divalent SAPs, absorption is caused by their difference in pore volume given by the ionic radii. The remarkable properties of NH_4^+ gel and SAP, compared to the other cations, are attributed to the ability of the ammonium cation to rotate, which increases the number of available carboxyl groups that engage in hydrogen bonding, resulting in an increase in pore area, gel stiffness and SAP swelling [51].

This study not only demonstrates the potential of nanocellulose-based SAPs with different cations to suit a range of applications but also innovates on the preparation method, that is by performing ion exchange before fibrillation -and not after- resulting in a cheaper and faster process than the conventional treatment. The addition of these cations can assist in the transition of the superabsorbent as a hydro-retentor to a nutrient carrier material, increasing the benefits of this material for agricultural and food use.

CRediT authorship contribution statement

Ruth M. Barajas-Ledesma: Conceptualization, Visualization, Methodology, Investigation, Software, Writing - original draft. **Laila Hossain:** Methodology, Software, Formal analysis, Writing - review & editing. **Vanessa N.L. Wong:** Supervision, Writing - review & editing. **Antonio F. Patti:** Supervision, Writing - review & editing. **Gil Garnier:** Visualization, Supervision, Writing - review & editing.

Declaration of Competing Interest

The authors declare that they have no known competing financial interests or personal relationships that could have appeared to influence the work reported in this paper.

Acknowledgement

Financial support was from the Australian Research Council (ARC), Norske Skog, Visy, the Government of Tasmania and Opal through the Industry Transformation Research Hub Processing Advance Lignocellulosics (PALS) grant IH130100016.

References

[1] E.M. Ahmed, Hydrogel: preparation, characterization, and applications: a review, J. Adv. Res. 6 (2) (2015) 105–121.
[2] S. Ghorbani, H. Eyni, S.R. Bazaz, H. Nazari, L.S. Asl, H. Zaferani, V. Kiani, A.A. Mehrizi, M. Soleimani, Hydrogels based on cellulose and its derivatives: applications, synthesis, and characteristics, Polym. Sci., Ser. A 60 (6) (2019) 707–722.
[3] X. Shen, J.L. Shamshina, P. Berton, G. Gurau, R.D. Rogers, Hydrogels based on cellulose and chitin: fabrication, properties, and applications, Green Chem. 18 (1) (2016) 53–75.
[4] J.R. Gross, The Evolution of Absorbent Materials, in: L. Brannon-Peppas, R.S. Harland (Eds.), Studies in Polymer Science, Elsevier, 1990, pp. 3–22.
[5] R. Curvello, V.S. Raghuwanshi, G. Garnier, Engineering nanocellulose hydrogels for biomedical applications, Adv. Colloid Interface Sci. 267 (2019) 47–61.
[6] H. Dong, J.F. Snyder, K.S. Williams, J.W. Andzelm, Cation-induced hydrogels of cellulose nanofibrils with tunable moduli, Biomacromolecules 14 (9) (2013) 3338–3345.
[7] J. Yang, F. Xu, C.-R. Han, Metal ion mediated cellulose nanofibrils transient network in covalently cross-linked hydrogels: mechanistic insight into morphology and dynamics, Biomacromolecules 18 (3) (2017) 1019–1028.
[8] N. Lavoine, L. Bergström, Nanocellulose-based foams and aerogels: processing, properties, and applications, J. Mater. Chem. A 5 (31) (2017) 16105–16117.
[9] K.J. De France, T. Hoare, E.D. Cranston, Review of hydrogels and aerogels containing nanocellulose, Chem. Mater. 29 (11) (2017) 4609–4631.
[10] L. Mendoza, L. Hossain, E. Downey, C. Scales, W. Batchelor, G. Garnier, Carboxylated nanocellulose foams as superabsorbents, J. Colloid Interface Sci. 538 (2019) 433–439.
[11] J. Grignon, A.M. Scallan, Effect of pH and neutral salts upon the swelling of cellulose gels, J. Appl. Polym. Sci. 25 (12) (1980) 2829–2843.
[12] A. Bashari, A. Rouhani Shirvan, M. Shakeri, Cellulose-based hydrogels for personal care products, Polym. Adv. Technol. 29 (12) (2018) 2853–2867.
[13] T.M. Neethu, P.K. Dubey, A.R. Kaswala, Prospects and applications of hydrogel technology in agriculture, Int. J. Curr. Microbiol. Appl. Sci. 7 (05) (2018) 3155–3162.
[14] R. Curvello, G. Garnier, Cationic cross-linked nanocellulose-based matrices for the growth and recovery of intestinal organoids, Biomacromolecules 22 (2) (2021) 701–709.
[15] M.J. Zohuriaan-Mehr, K. Kabiri, Superabsorbent polymer materials: a review, Iran. Polym. J. 17 (6) (2008) 451–477.
[16] M.R. Guilherme, F.A. Aouada, A.R. Fajardo, A.F. Martins, A.T. Paulino, M.F.T. Davi, A.F. Rubira, E.C. Muniz, Superabsorbent hydrogels based on polysaccharides for application in agriculture as soil conditioner and nutrient carrier: a review, Eur. Polym. J. 72 (2015) 365–385.
[17] Z. Steinmetz, C. Wollmann, M. Schaefer, C. Buchmann, J. David, J. Tröger, K. Muñoz, O. Frör, G.E. Schaumann, Plastic mulching in agriculture. Trading short-term agronomic benefits for long-term soil degradation?, Sci Total Environ. 550 (2016) 690–705.
[18] A.A. Horton, A. Walton, D.J. Spurgeon, E. Lahive, C. Svendsen, Microplastics in freshwater and terrestrial environments: evaluating the current understanding to identify the knowledge gaps and future research priorities, Sci. Total Environ. 586 (2017) 127–141.
[19] L. Ramos, G. Berenstein, E.A. Hughes, A. Zalts, J.M. Montserrat, Polyethylene film incorporation into the horticultural soil of small periurban production units in Argentina, Sci. Total Environ. 523 (2015) 74–81.
[20] P. Chen, W.A. Zhang, W. Luo, Y.e. Fang, Synthesis of superabsorbent polymers by irradiation and their applications in agriculture, J. Appl. Polym. Sci. 93(4) (2004) 1748-1755.
[21] M.R. Guilherme, A.V. Reis, A.T. Paulino, T.A. Moia, L.H.C. Mattoso, E.B. Tambourgi, Pectin-based polymer hydrogel as a carrier for release of agricultural nutrients and removal of heavy metals from wastewater, J. Appl. Polym. Sci. (2010) n/a-n/a.
[22] X. Shi, W. Wang, A. Wang, pH-responsive sodium alginate-based superporous hydrogel generated by an anionic surfactant micelle templating, Carbohydr. Polym. 94 (1) (2013) 449–455.
[23] A. Sannino, C. Demitri, M. Madaghiele, Biodegradable cellulose-based hydrogels: design and applications, Materials 2 (2) (2009) 353–373.
[24] J. De Guzman, K. Dela Peña, J. Ytac Dorothy, T. Tumolva, Synthesis and characterization of ionically-crosslinked κ- carrageenan/sodium alginate/carboxymethyl cellulose hydrogel blends for soil water retention and fertilizer release, Solid State Phenom. 304 (2020) 59–65.
[25] S. Varanasi, R. He, W. Batchelor, Estimation of cellulose nanofibre aspect ratio from measurements of fibre suspension gel point, Cellulose 20 (4) (2013) 1885–1896.
[26] A. Isogai, T. Saito, H. Fukuzumi, TEMPO-oxidized cellulose nanofibers, Nanoscale 3 (1) (2011) 71–85.
[27] Z. Pakowski, Modern methods of drying nanomaterials, Transp. Porous Media 66 (1–2) (2006) 19–27.
[28] E. Bresler, Saline and Sodic Soils Principles-Dynamics-Modeling, 1st ed, Berlin, Heidelberg : Springer Berlin Heidelberg : Imprint: Springer, 1982.
[29] I. Homma, H. Fukuzumi, T. Saito, A. Isogai, Effects of carboxyl-group counter-ions on biodegradation behaviors of TEMPO-oxidized cellulose fibers and nanofibril films, Cellulose 20 (5) (2013) 2505–2515.
[30] H. Dong, J.F. Snyder, D.T. Tran, J.L. Leadore, Hydrogel, aerogel and film of cellulose nanofibrils functionalized with silver nanoparticles, Carbohydr. Polym. 95 (2) (2013) 760–767.
[31] M. Chau, S.E. Sriskandha, D. Pichugin, H. Thérien-Aubin, D. Nykypanchuk, G. Chauve, M. Méthot, J. Bouchard, O. Gang, E. Kumacheva, Ion-mediated gelation of aqueous suspensions of cellulose nanocrystals, Biomacromolecules 16 (8) (2015) 2455–2462.
[32] L. Mendoza, W. Batchelor, R.F. Tabor, G. Garnier, Gelation mechanism of cellulose nanofibre gels: a colloids and interfacial perspective, J. Colloid Interface Sci. 509 (2018) 39–46.
[33] S. Ang, V. Haritos, W. Batchelor, Cellulose nanofibers from recycled and virgin wood pulp: a comparative study of fiber development, Carbohydr. Polym. 234 (2020) 115900.
[34] T. Saito, A. Isogai, TEMPO-mediated oxidation of native cellulose. The effect of oxidation conditions on chemical and crystal structures of the water-insoluble fractions, Biomacromolecules 5 (5) (2004) 1983–1989.
[35] M. Maliha, M. Herdman, R. Brammananth, M. McDonald, R. Coppel, M. Werrett, P. Andrews, W. Batchelor, Bismuth phosphinate incorporated nanocellulose sheets with antimicrobial and barrier properties for packaging applications, J. Cleaner Prod. 246 (2020) 119016.
[36] D.J. Mendoza, L. Hossain, C. Browne, V.S. Raghuwanshi, G.P. Simon, G. Garnier, Controlling the transparency and rheology of nanocellulose gels with the extent of carboxylation, Carbohydr. Polym. 245 (2020) 116566.
[37] R. Prathapan, R. Thapa, G. Garnier, R.F. Tabor, Modulating the zeta potential of cellulose nanocrystals using salts and surfactants, Colloids Surf., A 509 (2016) 11–18.
[38] I. Besbes, S. Alila, S. Boufi, Nanofibrillated cellulose from TEMPO-oxidized eucalyptus fibres: effect of the carboxyl content, Carbohydr. Polym. 84 (3) (2011) 975–983.
[39] O. Nechyporchuk, M.N. Belgacem, F. Pignon, Current progress in rheology of cellulose nanofibril suspensions, Biomacromolecules 17 (7) (2016) 2311–2320.
[40] IUPAC, Compendium of Chemical Terminology, second ed. (the "Gold Book"), Blackwell Scientific Publications, Oxford, 1997.
[41] T. Saito, T. Uematsu, S. Kimura, T. Enomae, A. Isogai, Self-aligned integration of native cellulose nanofibrils towards producing diverse bulk materials, Soft Matter 7 (19) (2011) 8804–8809.
[42] J.N. Israelachvili, Intermolecular and surface forces, third ed., Academic Press, Burlington, Massachusetts, 2011.
[43] E. Joseph, G. Singhvi, Chapter 4 - multifunctional nanocrystals for cancer therapy: a potential nanocarrier, in: A.M. Grumezescu (Ed.), Nanomaterials for Drug Delivery and Therapy, William Andrew Publishing, 2019, pp. 91–116.
[44] A.B. Fall, S.B. Lindström, O. Sundman, L. Ödberg, L. Wågberg, Colloidal stability of aqueous nanofibrillated cellulose dispersions, Langmuir 27 (18) (2011) 11332–11338.
[45] T. Oncsik, G. Trefalt, M. Borkovec, I. Szilagyi, Specific ion effects on particle aggregation induced by monovalent salts within the hofmeister series, Langmuir 31 (13) (2015) 3799–3807.
[46] H. Huang, E. Ruckenstein, Effect of hydration of ions on double-layer repulsion and the hofmeister series, J. Phys. Chem. Lett. 4 (21) (2013) 3725–3727.
[47] E. Ruckenstein, H. Huang, Specific ion effects on double layer forces through ion hydration, Colloids Surf., A 459 (2014) 151–156.
[48] R.M. Barajas-Ledesma, A.F. Patti, V.N.L. Wong, V.S. Raghuwanshi, G. Garnier, Engineering nanocellulose superabsorbent structure by controlling the drying rate, Colloids Surf., A 600 (2020) 124943.
[49] R.D. Shannon, Revised effective ionic radii and systematic studies of interatomic distances in halides and chalcogenides, Acta Crystallogr. Sect. A 32 (5) (1976) 751–767.
[50] J. Guo, L. Zhou, A. Zen, A. Michaelides, X. Wu, E. Wang, L. Xu, J. Chen, Hydration of NH4+ in water: bifurcated hydrogen bonding structures and fast rotational dynamics, Phys. Rev. Lett. 125 (10) (2020) 106001.
[51] Z. Xia, M. Patchan, J. Maranchi, J. Elisseeff, M. Trexler, Determination of crosslinking density of hydrogels prepared from microcrystalline cellulose, J. Appl. Polym. Sci. 127 (6) (2013) 4537–4541.